Electronic Supplementary Information

Biocompatible small organic molecule phototheranostics for NIR-II fuorescence/photoacoustic imaging and simultaneous photodynamic/photothermal combination therapy

Qi Wang,[a] Bing Xia,[a] Jingzeng Xu,[a] Xinrui Niu,[a] Jie Cai,[a] Qingming Shen,[a] Wenjun Wang,[b] Wei Huang[a,c] and Quli Fan*[,a,c]

[a] *Key Laboratory for Organic Electronics and Information Displays & Jiangsu Key Laboratory for Biosensors, Institute of Advanced Materials (IAM), Jiangsu National Synergetic Innovation Center for Advanced Materials (SICAM), Nanjing University of Posts & Telecommunications, Nanjing 210023, China. E-mail: iamqlfan@njupt.edu.cn*

[b] *Key Lab of Optical Communication Science and Technology of Shandong Province & School of Physics Science and Information Engineering, Liaocheng University, Liaocheng 252059, China*

[c] *Shaanxi Institute of Flexible Electronics (SIFE), Northwestern Polytechnical University (NPU), 127 West Youyi Road, Xi'an 710072, China*

Table of Contents

1. General information and experimental procedure

General information

All reactions were performed in atmosphere unless noted. The commercially available reagents and solvents were either employed as purchased or dried according to procedures described in the literature. Compounds 1,[S1] and 2,[S2] were prepared according to literature procedure. NMR spectra were carried out on a 400 MHz NMR spectrometer (Ultra Shield Plus, Bruker). The morphology and size of NPs were determined by a HT7700 transmission electron microscope (TEM) and a particle size analyzer (Brookhaven Instruments), respectively. Absorption and emission spectra were obtained using a UV3600 UV/vis/NIR spectrophotometer (Shimadzu) and a FLSP920 fluorescence spectrophotometer (Edinburgh), respectively. The MTT experiments were conducted using a PowerWave XS/XS2 microplate reader (BioTek).

Experimental procedure

Preparation of DPP-BDT NPs: DPP-BDT in THF (2.0 mg/mL, 1 mL) was quickly added into the aqueous solution (4 mL) of DSPE-mPEG5000 (10 mg) under sonication. Then, THF was dislodged via argon blowing at surface of solution. Water-soluble DPP-BDT NPs were obtained after filtered.

Photothermal measurement of DPP-BDT NPs: the temperature changes of DPP-BDT NPs with different concentrations (0, 20, 40, 60, 80, and 100 μg/mL) under 660 nm laser (0.75 W/cm^2) were acquired by an IR image camera (FLIR E50; Estonia). In addition, 100 μg/mL DPP-BDT NPs under irradiation with 660 nm laser at various power densities (0.3, 0.5, 0.75, and 1.0 W/cm^2) were also studied.

Photodynamic measurement of DPP-BDT NPs: DPBF in ethanol (2×10^{-5} mol/L) was added into DPP-BDT NPs aqueous solution (1×10^{-5} mol/L, 2 mL). The samples were exposed to 660 nm laser with various power densities, and the absorption spectra at different time points were acquired by a UV/vis/NIR spectrophotometer.

In vitro cell assay: *in vitro* cell cytotoxicity of DPP-BDT NPs against NIH-3T3 cells and Hela cells were evaluated by MTT assay. Hela tumor cells and NIH-3T3

normal cells (1×10^6 cells/well) were cultured in DMEM medium with 10% fetal bovine serum and 1% streptomycin/penicillin at 37 °C in 5% CO_2 for 24 h. Then, NIH-3T3 cells were treated in fresh medium with DPP-BDT NPs. Hela cells were treated in fresh medium with DPP-BDT NPs, and divided into two groups: (1) without irradiation, (2) with 660 nm laser irradiation (0.75 W/cm^2, 10 min). After 24 h of co-cultivation, MTT (20 μL) was added into each well and further culturing for another 3 h. Next, the formed formazans were dissolved with DMSO after removed the supernatant, and the absorbance was monitored by microplate reader with untreated cells as control.

Live and dead cell assay: HeLa cells were treated with the same ways as above and co-stained with 1 μM Calcein AM (for live cells) and 4 μM PI (for dead cells) for 10 min. Fluorescence images of cells were obtained under an inverted fluorescence microscope. The red fluorescence for PI was collected at the emission of 590 nm with the excitation at 540-580 nm, the green fluorescence for Calcein AM was collected at 510-550 nm with excitation at 470-490 nm.

In vitro NIR-II fluorescence imaging and PA imaging: for NIR-II imaging, the fluorescence imaging of DPP-BDT NPs with different concentrations (0.04375, 0.0875, 0.175, 0.25, and 0.5 mg/mL) was recorded by an NIR-II fluorescence imaging instrument. For PAI, DPP-BDT NPs with different concentrations (0.0625, 0.125, 0.25, 0.5, 1, and 2 mg/mL) were added into 600 μL agar tubes for PA signal detection using a PA instrument (Nexus 128, Endra Inc.).

In vivo NIR-II fluorescence imaging and PA imaging: for *in vivo* NIR-II imaging, after tail vein injection of DPP-BDT NPs (200 μL, 2 mg/mL) into Hela tumor-bearing mice, the real-time NIR-II imaging was acquired using a home built NIR-II fluorescence imaging instrument at 0, 4, 12, 20, 48, and 72 h postinjection. For *in vivo* PA imaging, the mice were monitored by a PA instrument (Nexus 128, Endra Inc.) at indicated time points after injection.

In vivo combination therapy: in order to investigate the combination therapy effect of DPP-BDT NPs in vivo, Hela tumor-bearing mice were stochastically divided into four groups and given following treatments: (1) control group without any treatment,

(2) NIR laser only, (3) DPP-BDT NPs only (2 mg mL^{-1}, 150 μL), (4) DPP-BDT NPs (2 mg mL^{-1}, 150 μL) + laser. After 20 h postinjection of NPs, the tumor areas of the mice were exposed to a 660 nm laser (1 W/cm^2) for 10 min. Then, the tumor volume and body weight of the mice were recorded every two days within 14 days. After therapy, the mice were dissected, and the final tumor and major organs were further studied by H&E staining.

2. *Synthesis of small-molecule NIR-II dye DPP-BDT*

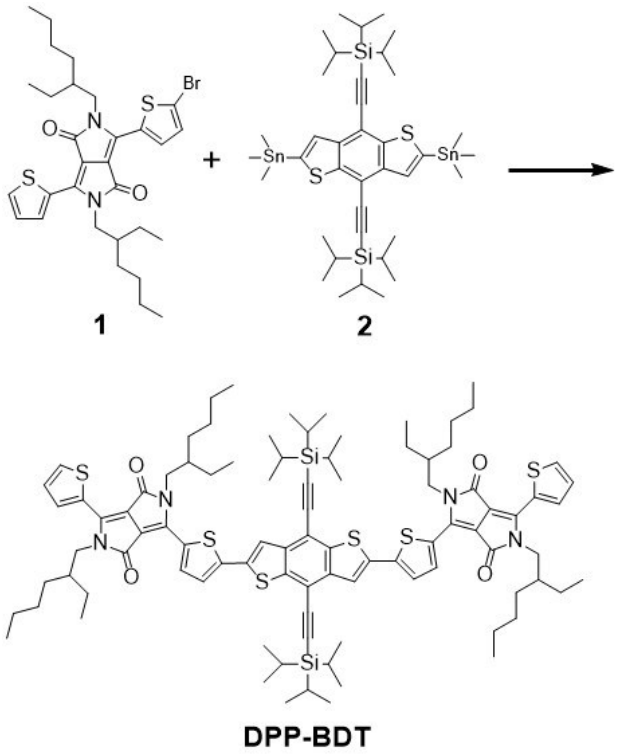

Scheme S1 Synthesis of DPP-BDT.

Compound 1 (0.21g, 0.34 mmol), compound 2 (0.15 g, 0.17 mmol), $Pd(PPh_3)_4$ (15mg), and anhydrous toluene (20 mL) were mixed in a round-bottom flask under argon atmosphere. The mixture was vigorously stirred at 110 °C for 24 h. After removal of the solvent, the crude product was purified by column chromatography to obtain DPP-BDT as a blue-black solid (0.14g, 0.09 mmol, 53%). ^{1}H NMR (400 MHz, $CDCl_3$, 298 K) δ (ppm): 8.97 (d, 2H), 8.91 (d, 2H), 7.77 (s, 2H), 7.64 (d, 2H), 7.50 (d, 2H), 7.28 (t, 2H), 4.04 (t, 8H), 1.98 (br, s, 4H), 1.30-1.21 (m, 66H), 0.86-0.83 (m, 32H). ^{13}C NMR (100 MHz, $CDCl_3$, 298 K) δ (ppm): 161.8, 142.0, 140.9, 140.7, 139.7, 139.6, 137.9, 136.8, 135.6, 130.9, 130.1, 129.9, 128.6, 126.9, 120.5, 111.9, 109.0, 108.4, 103.4, 102.0, 46.6, 46.5, 37.9, 32.0, 31.1, 30.9, 29.9, 28.6, 28.5, 26.34, 26.25, 23.2, 22.8, 19.03, 18.97, 14.24, 14.20, 11.6, 11.5. LR-ESI-MS: *m*/*z* calcd. for $[M + NH_4]^+$ = 1614.58, found 1614.60 (100%).

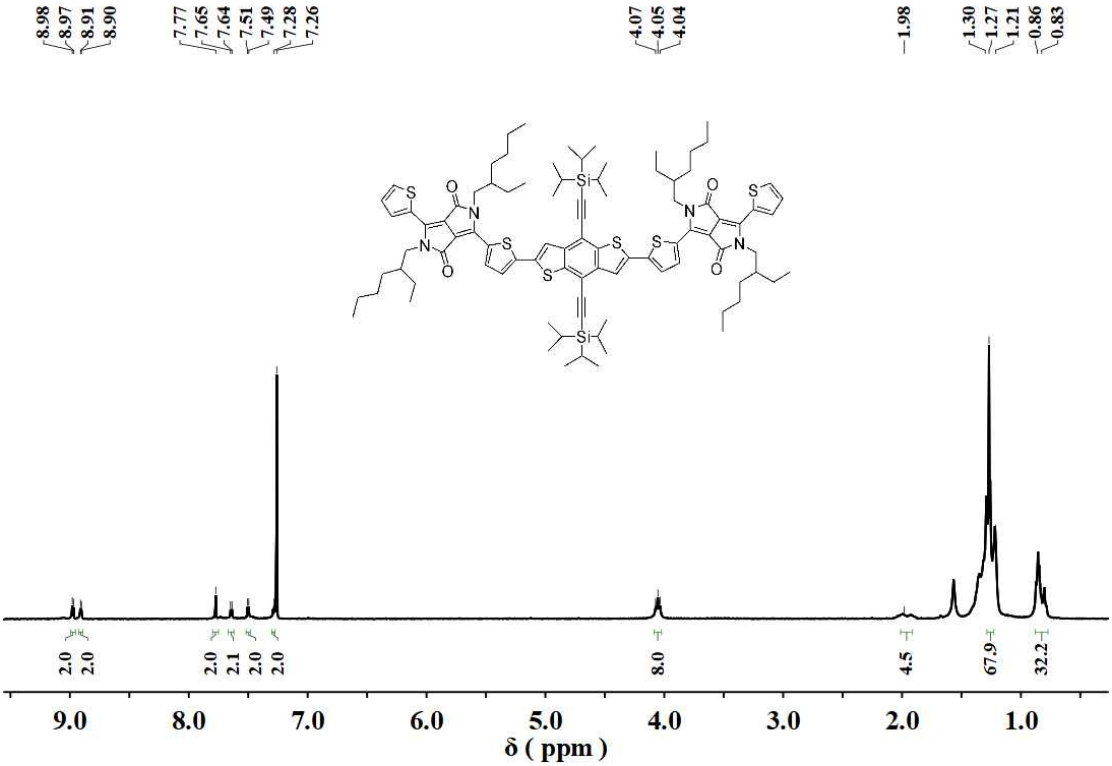

Fig. S1 ^{1}H NMR spectrum (400 MHz, $CDCl_3$, 298 K) of DPP-BDT.

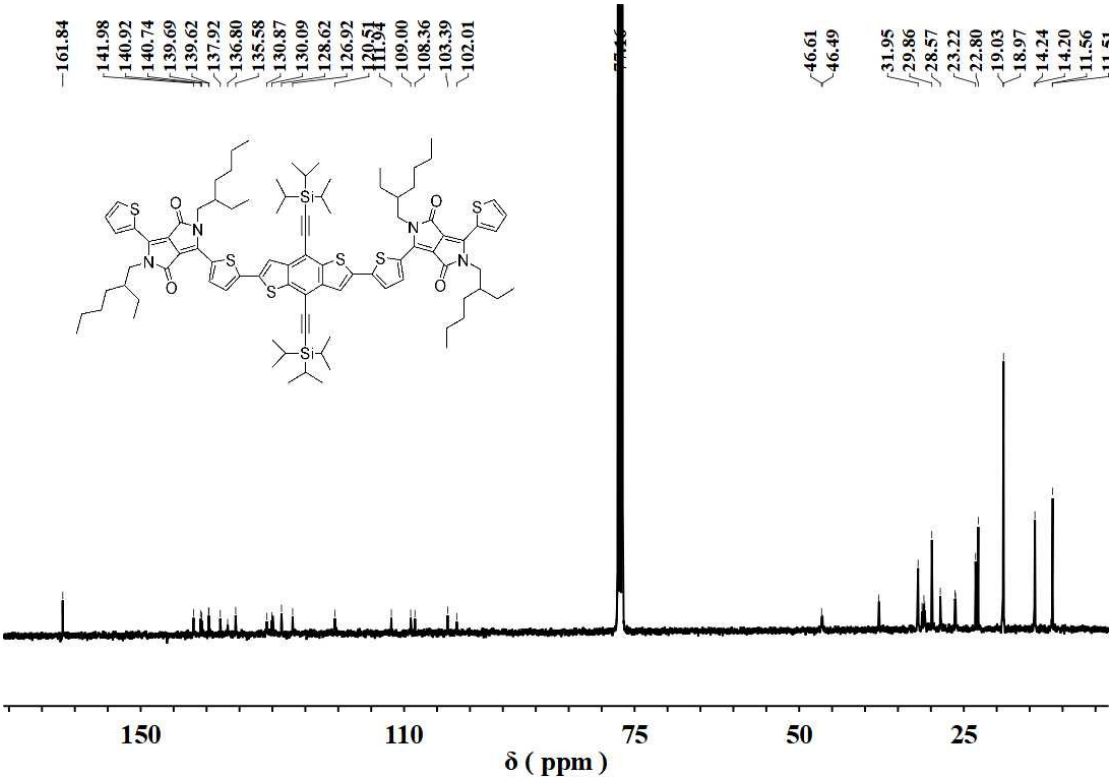

Fig. S2 ^{13}C NMR spectrum (100 MHz, $CDCl_3$, 298 K) of DPP-BDT.

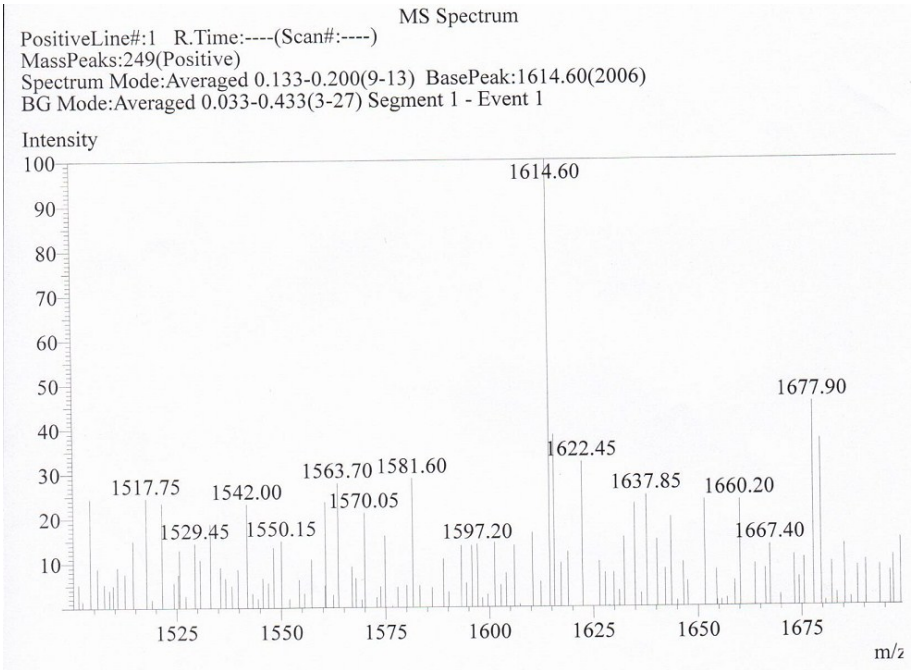

Fig. S3 LR-ESI-MS spectrum of DPP-BDT.

3. *Stability of DPP-BDT NPs*

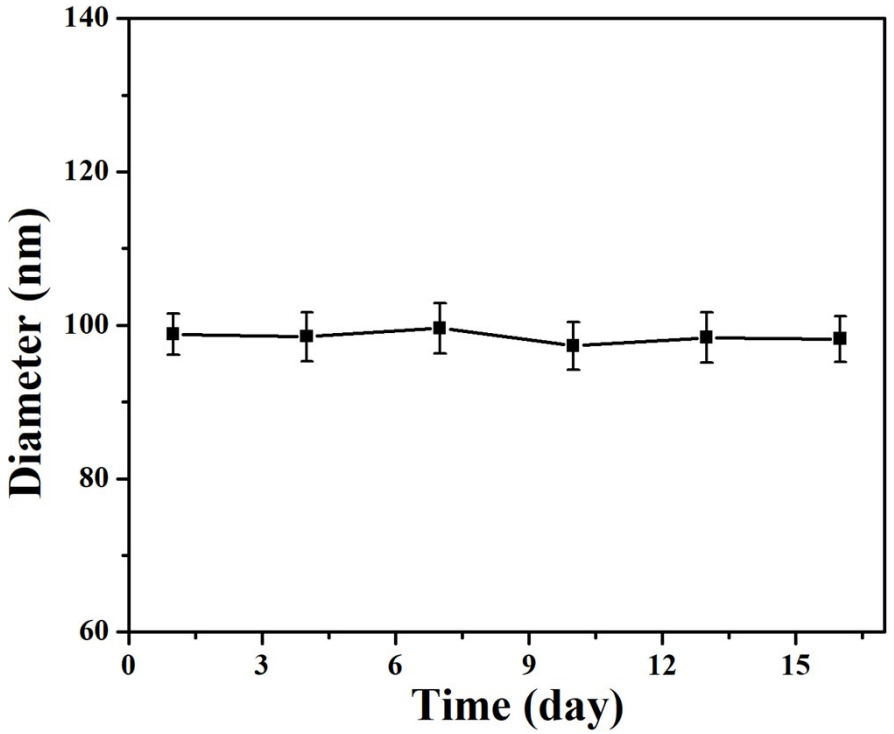

Fig. S4 Stability of DPP-BDT NPs with different time.

4. *UV-Vis-NIR absorption of DPP-BDT NPs in water*

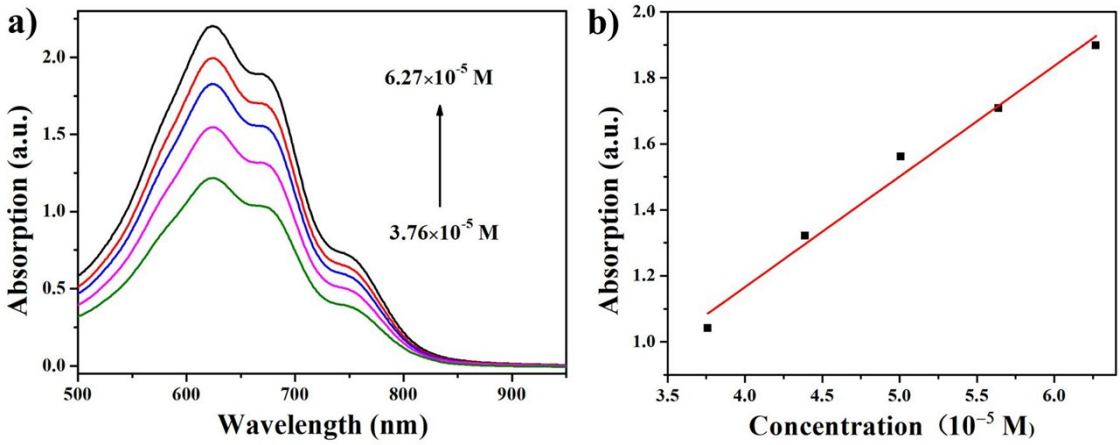

Fig. S5 (a) Absorption curves of DPP-BDT NPs at different concentrations. (b) Linear absorbance versus concentration obtained from (a).

5. *Photostability comparison of DPP-BDT NPs with MB*

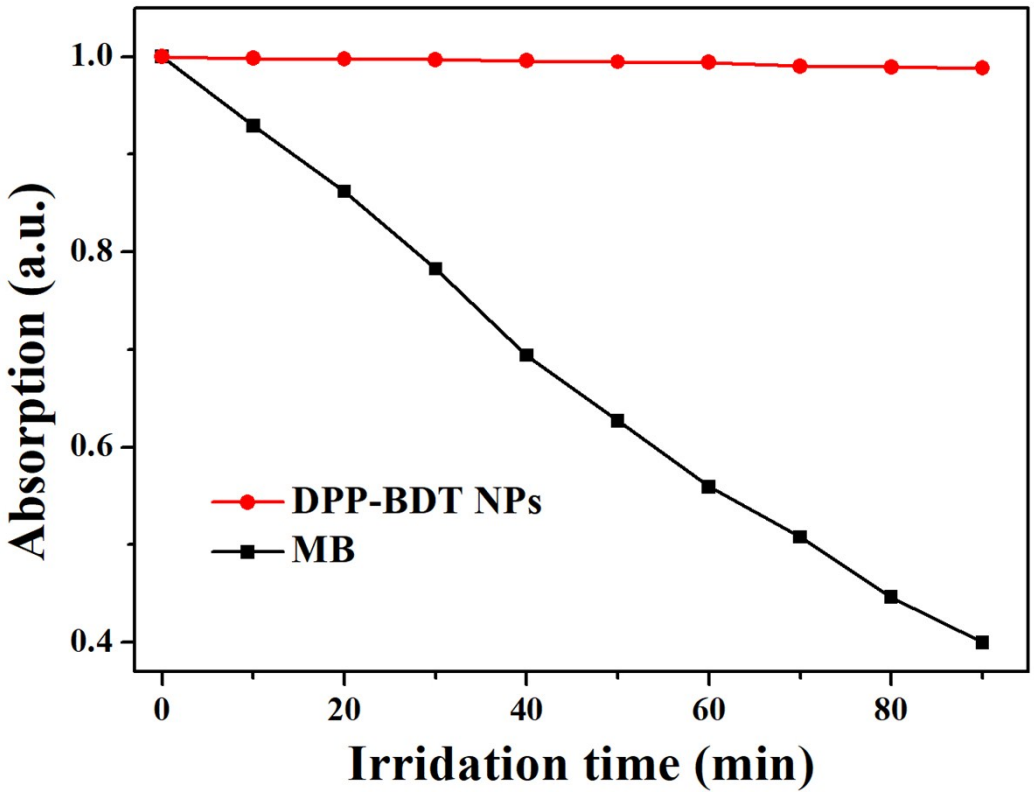

Fig. S6 Photostability comparison of DPP-BDT NPs with MB.

6. *Penetration depth measurement of DPP-BDT NPs*

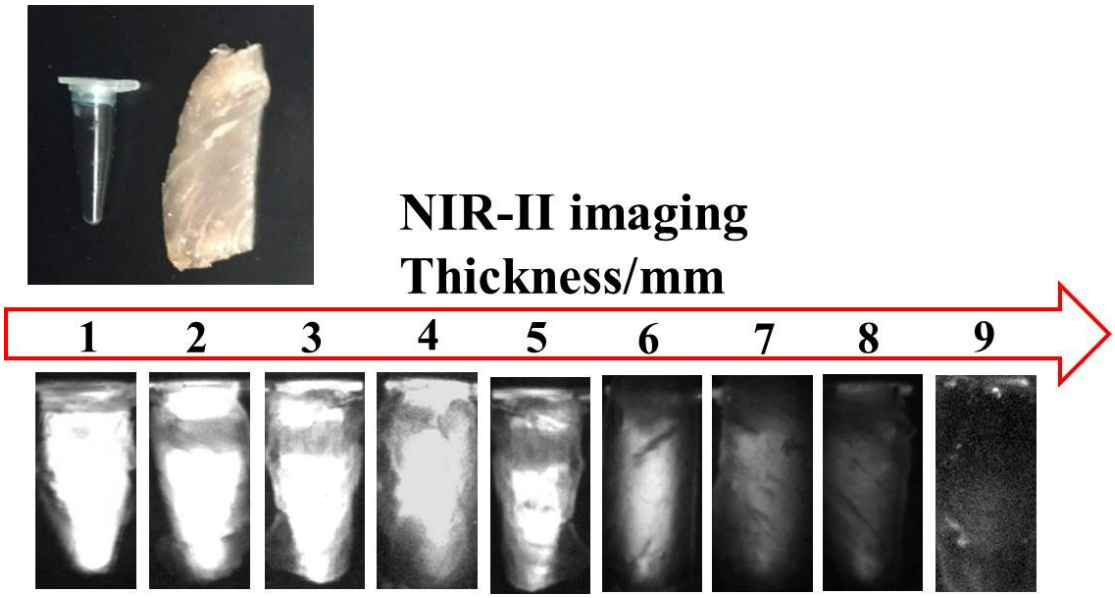

Fig. S7 Penetration depth measurement of DPP-BDT NPs in a simulated deep-tissue setting (chicken-breast tissues).

7. *Infrared thermal images of DPP-BDT NPs*

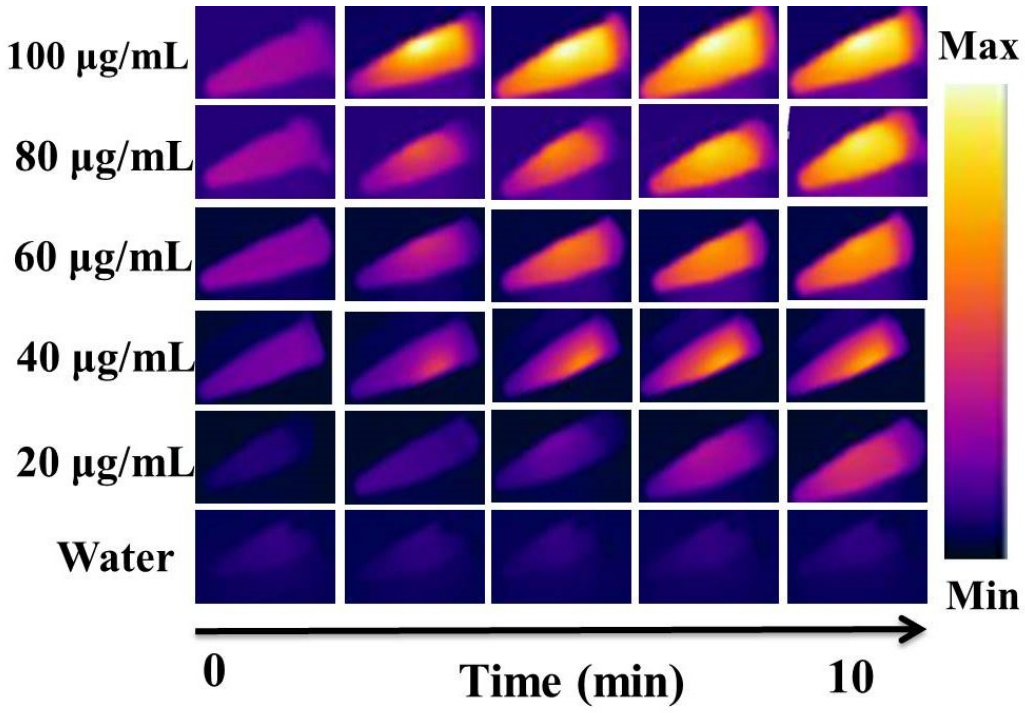

Fig. S8 Infrared thermal images of DPP-BDT NPs in water after NIR laser irradiation for different times (660 nm, 0.75 W/cm^2).

8. *Photothermal stability of DPP-BDT NPs*

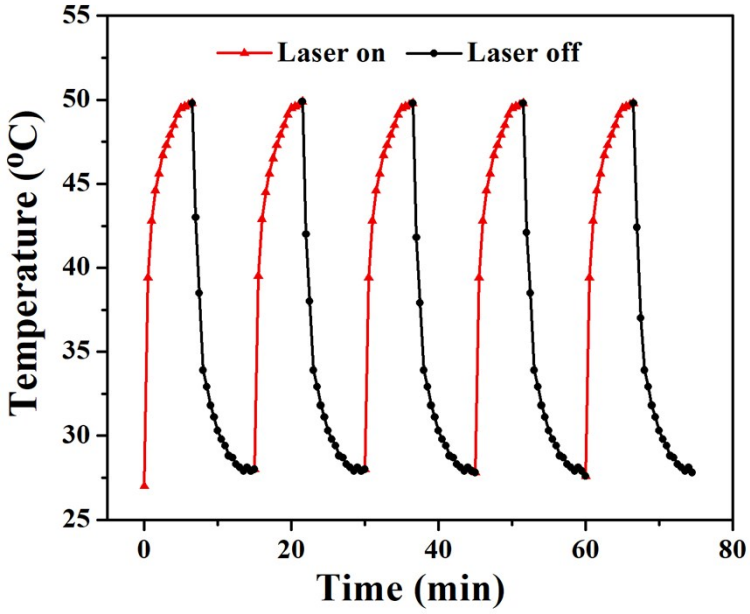

Fig. S9 Photothermal stability of DPP-BDT NPs.

9. *Photothermal conversion efficiency measurement of DPP-BDT NPs*

For calculating the photothermal conversion efficiency (η) of DPP-BDT NPs, DPP-BDT NPs solution was irradiated by a 660 nm laser (1.0 W/cm^2) for 6 min, then the laser was shut off. After reaching a plateau temperature, the solution was naturally cooled to room temperature without NIR laser irradiation. And the temperature was recorded by IR thermal camera. Deionized water of the same volume was used as control.

The η was calculated by equation:[S5]

$$\eta = \frac{\mathrm{hs}(T_{\max} - T_{\mathrm{surr}}) - Q_0}{I(1-10^{-A_\lambda})} \qquad (1)$$

hs can be calculated by the follow equation:

$$\mathrm{hs} = \frac{\sum m_i C_{P.i}}{\tau_s} \qquad (2)$$

$$\tau_s = \frac{t}{-\ln\theta} \qquad (3)$$

$$\theta = \frac{T - T_{surr}}{T_{max} - T_{surr}} \qquad (4)$$

$$Q_0 = hs(T_{max} - T_{surr}) \qquad (5)$$

h represents the heat transfer coefficient,

s represents the sample container surface area,

T_{max} represents the steady-state maximum temperature,

T_{surr} represents the ambient room temperature,

T represents instantaneous temperature during cooling,

t represents the time it takes by T cooled to room temperature,

C approximate to the specific heat capacity of water,

m represented the mass of the solution (g),

Q_0 represents the energy input by the same solvent without NPs in the same quartz cuvette after same laser irradiation.

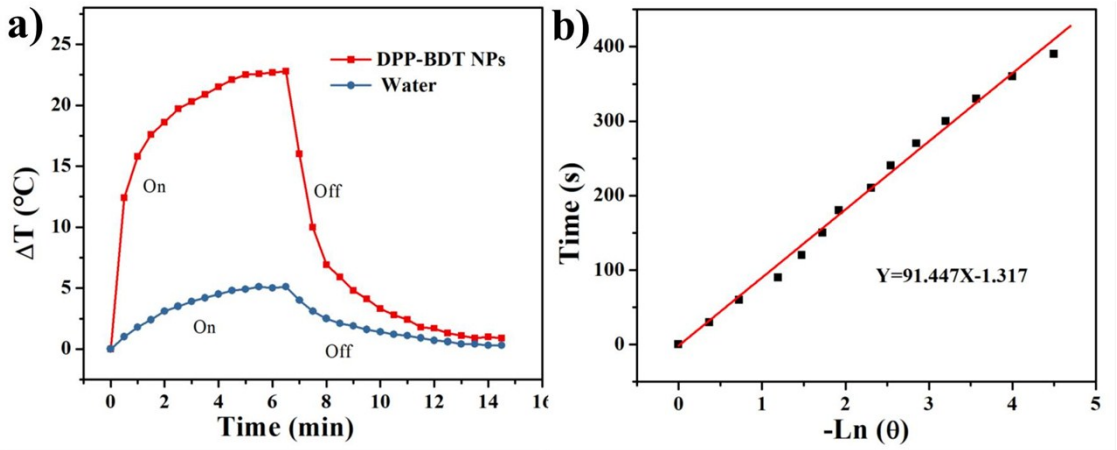

Fig. S10 a) The heating curve of the DPP-BDT NP aqueous dispersion in a procedure of laser-on and off (pure water was irradiated as a control). (b) The linear cooling time data versus -ln(θ) obtained from the cooling period of a).

10.$^1O_2$ quantum yield measurement of DPP-BDT NPs

Singlet oxygen quantum yield was calculated by $\Phi_{\Delta(X)} = \Phi_{\Delta(MB)} \times (S_X/S_{MB}) \times (F_{MB}/F_X)$, in which the subscripts X and MB represent DPP-BDT NPs and methylene blue, respectively. S represents slope of absorbance plot of DPBF (414 nm) vs irradiation time. F represents absorption correction factor calculated by $F = 1\text{-}10^{-OD}$ (OD represents absorbance of the DPP-BDT NPs and methylene blue at 660 nm).

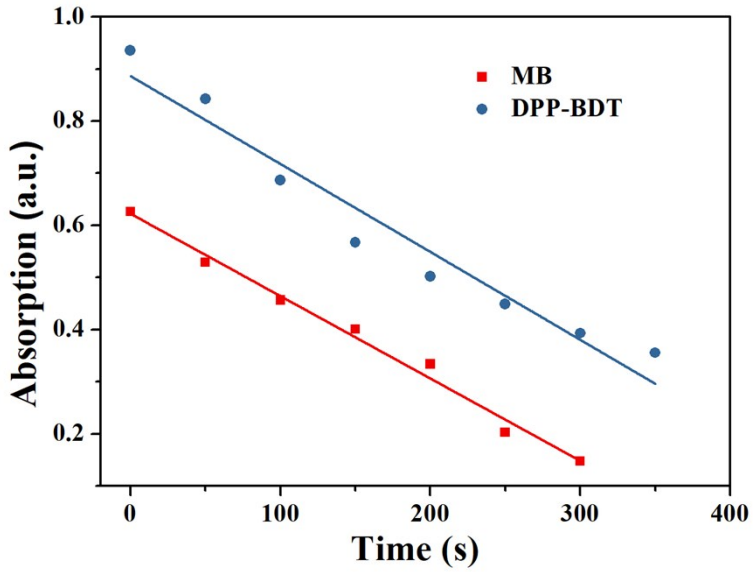

Fig. S11 $^1O_2$ generation from a plot of changes in absorbance by DPBF at 414 nm against different irradiation time (with 660 nm laser) in the presence of DPP-BDT NPs in water with methylene blue (MB) as a standard.

11.Ex vivo NIR-II fluorescence images of major organs and tumors

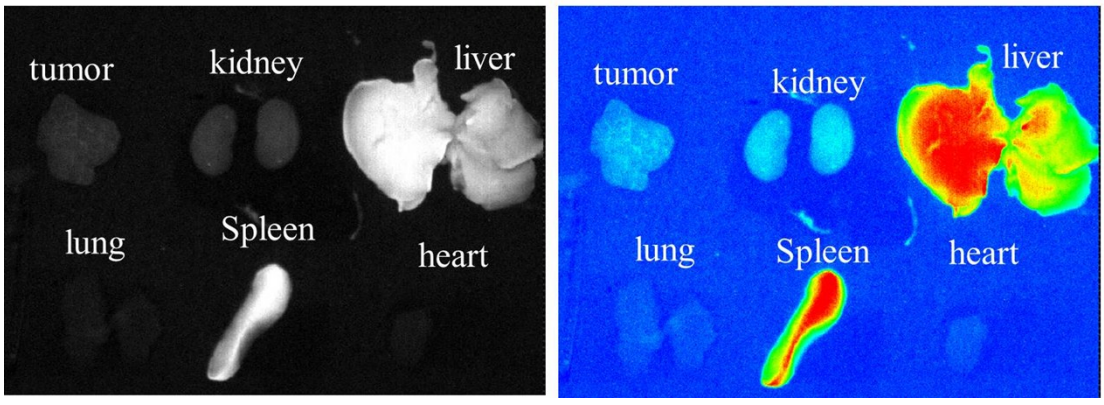

Fig. S12 *Ex vivo* NIR-II fluorescence images of dissected tumor and major organs after injection of DPP-BDT NPs.

12.Infrared thermal imaging of DPP-BDT NPs in vivo

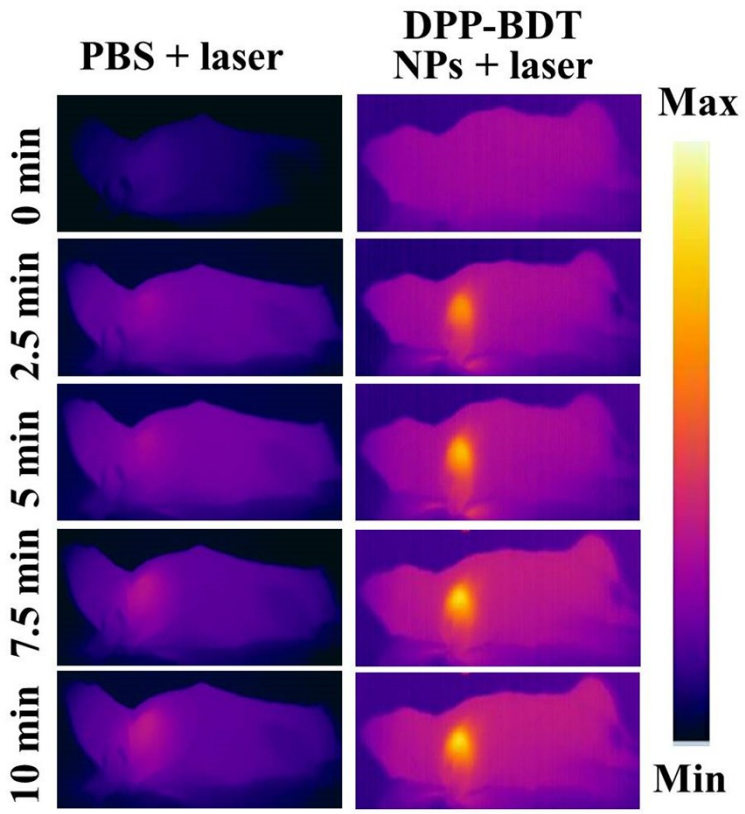

Fig. S13 Infrared thermal imaging of DPP-BDT NPs *in vivo*.

References:

S1. J. Liu, Y. Sun, P. Moonsin, M. Kuik, C. M. Proctor, J. Lin, B. B. Hsu, V. Promarak, A. J. Heeger and T.-Q. Nguyen, *Adv. Mater.*, 2013, **25**, 5898-5903.

S2. H. G. Kim, S. B. Jo, C. Shim, J. Lee, J. Shin, E. C. Cho, S.-G. Ihn, Y. S. Choi, Y. Kim and K. Cho, *J. Mater. Chem.*, 2012, **22**, 17709-17717.

S3 Z. Tao, G. Hong, C. Shinji, C. Chen, S. Diao, A. L. Antaris, B. Zhang, Y. Zou, H. Dai, *Angew. Chem. Int. Ed.*, 2013, **52**, 13002-13006.

S4 G. Hong, Y. Zou, A. L. Antaris, S. Diao, D. Wu, K. Cheng, X. Zhang, C. Chen, B. Liu, Y. He, J. Z. Wu, J. Yuan, B. Zhang, Z. Tao, C. Fukunaga, H. Dai, *Nat. Commun.*, 2014, **5**, 4206.

S5. P.Liang, Q.Tang, Y.Cai, G.Liu, W. Si, J.Shao, W. Huang, Q. Zhang and X. Dong, *Chem. Sci.*, 2017, **8**, 7457-7463.